



HAL
open science

Nickel-Decorated Silver Nanowires for Polymer-Based Magnetoelectric Composite

Baptiste Martin, Eric Dantras, Antoine Lonjon, Lydia Laffont, Colette
Lacabanne

► **To cite this version:**

Baptiste Martin, Eric Dantras, Antoine Lonjon, Lydia Laffont, Colette Lacabanne. Nickel-Decorated Silver Nanowires for Polymer-Based Magnetoelectric Composite. *physica status solidi (a)*, 2021, 218 (14), pp.2100037. 10.1002/pssa.202100037 . hal-03274801

HAL Id: hal-03274801

<https://hal.science/hal-03274801>

Submitted on 30 Jun 2021

HAL is a multi-disciplinary open access archive for the deposit and dissemination of scientific research documents, whether they are published or not. The documents may come from teaching and research institutions in France or abroad, or from public or private research centers.

L'archive ouverte pluridisciplinaire **HAL**, est destinée au dépôt et à la diffusion de documents scientifiques de niveau recherche, publiés ou non, émanant des établissements d'enseignement et de recherche français ou étrangers, des laboratoires publics ou privés.



Open Archive Toulouse Archive Ouverte (OATAO)

OATAO is an open access repository that collects the work of Toulouse researchers and makes it freely available over the web where possible

This is an author's version published in: <http://oatao.univ-toulouse.fr/27938>

Official URL: <https://doi.org/10.1002/pssa.202100037>

To cite this version:

Martin, Baptiste  and Dantras, Eric  and Lonjon, Antoine  and Laffont, Lydia  and Lacabanne, Colette  *Nickel-Decorated Silver Nanowires for Polymer-Based Magnetoelectric Composite*. (2021) *Physica Status Solidi A*. 2100037. ISSN 1862-6300

Any correspondence concerning this service should be sent to the repository administrator: tech-oatao@listes-diff.inp-toulouse.fr

Nickel-Decorated Silver Nanowires for Polymer-Based Magnetolectric Composite

Baptiste Martin, Eric Dantras,* Antoine Lonjon, Lydia Laffont, and Colette Lacabanne

Polymer-based magnetolectric composites are processed with an intrinsic piezoelectric poly(vinylidene fluoride-co-trifluoroethylene) (P(VDF-TrFE)) matrix and high-aspect-ratio magnetic nickel-decorated silver nanowires. These core/shell wires are obtained by the polyol reduction of Ni^{2+} ions on high-aspect-ratio silver nanowires. Scanning electron microscopy and transmission electron microscopy analyses show a homogeneous and well-crystallized nickel layer. Magnetic properties of the intrinsic particles and their composites are measured and show a strong enhancement of the coercive field compared to spherical Ni nanopowders. They also show the existence of strong magnetic anisotropy in the composites. The composites processed with a small amount of metallic particles (0.3 vol%) allow the maintaining of the P(VDF-TrFE) crystalline phase and the ability of a macroscopic polarization. The latter is conducted under a 80 MV m^{-1} field, leading to a significant d_{33} (3.2 pC N^{-1}). Thus, the magnetolectric properties are analyzed and an important coupling coefficient α_{ME} equal to $1.8 \text{ V m}^{-1} \text{ Oe}^{-1}$ is measured.

1. Introduction

Among physical couplings, magnetolectricity takes a special place. Despite the fact that its theory was formulated in crystals by Pierre Curie in 1894,^[1] it is one of the couplings that depend mostly on the realization of composites for their applications. The first experimental results on intrinsic magnetolectric materials were only made in 1961 by Astrov^[2] in chromium oxide at very low temperature. The major advance that opened the door for large applications was the idea of the extrinsic magnetolectric effect by mixing a piezoelectric and a ferromagnetic material.^[3] The principle is based on the dispersion of magnetic particles such as ferrites in a piezoelectric matrix such as BaTiO_3 .^[4,5] Discovery of polymeric

piezoelectric materials allowed new possibilities for magnetolectric composites in terms of processing. The principle remains the same but instead of a brittle inorganic matrix, a resilient polymer is used. The most common piezoelectric polymers are linear fluorinated polymer β -PVDF and poly(vinylidene fluoride-co-trifluoroethylene) (P(VDF-TrFE)) because of their excellent piezoelectric coefficients. These polymers have shown their interest through many applications such as energy harvesting,^[6] piezoelectricity,^[7] sensors,^[8] actuators, and high-frequency devices. Among these applications, magnetolectricity has taken an important place through the fabrication of hybrid composites.^[9–11] Thus, Nan et al. made the first polymer-based magnetolectric composites^[12] by dispersing magnetic particles of Terfenol-D in β -PVDF.

Previous studies have shown the preeminent role of magnetic particles in enhancing magnetolectric coupling through enhanced magnetic properties. Consequently, different ferrites such as NiFe_2O_4 ,^[13] Fe_3O_4 ,^[14] CoFe_2O_4 ,^[15] and MnFe_2O_4 ^[16] have been studied. Some authors have also reported a magnetolectric coupling with nickel particles in P(VDF-TrFE)^[17] and in three-phased magnetolectric composites.^[18,19] In comparison with ferrites, nickel exhibits higher remnant magnetization at ambient temperature, which can be interesting to improve the magnetolectric coupling in the composites. The main drawback of using metal instead of ceramics is the increase of the conductivity; it makes the poling of the matrix harder and then decreases the piezoelectric coefficient (d_{33}), especially for P(VDF-TrFE), which displays a high poling field 70 MV m^{-1} . In contrast, it has been widely shown that metallic magnetic particles exhibit enhanced magnetic properties depending on their shape.^[20,21] As widely reported in the literature, nickel appears to be a good candidate as it can be processed with various morphologies, such as wires and dumbbells.^[22,23] One of the key factors is the aspect ratio ξ . Thus, some works have been led by electrodeposited nickel nanowires (Ni NWs with $\xi = 250$ ^[24]) showing enhanced magnetic properties. Very good results have been shown but with an important process drawback: The reduction synthesis does not allow an important amount of Ni NWs. Independently, we mastered an easier process to synthesize a large amount of high- ξ silver wires (Ag NWs, $\xi \approx 250$).^[25,26] To combine the large amount of high- ξ silver wires and the good magnetic properties of nickel, we present

Dr. B. Martin, Dr. E. Dantras, Dr. A. Lonjon, Prof. C. Lacabanne
CIRIMAT
Physique des Polymères
Université de Toulouse
118 route de Narbonne, 31062 Toulouse cedex 09, France
E-mail: eric.dantras@univ-tlse3.fr

Dr. L. Laffont
CIRIMAT
ENSACET
Université de Toulouse
4 allée Emile Monso, CS44362, 31030 Toulouse, France

 The ORCID identification number(s) for the author(s) of this article can be found under <https://doi.org/10.1002/pssa.202100037>.

DOI: 10.1002/pssa.202100037

here a polyol route to decorate silver nanowires with nickel. The final aim of this work is to produce a high amount of high-aspect-ratio nickel-decorated silver nanowires for the fabrication of polymer-based magnetoelectric composites and study the influence of the morphology over the magnetoelectric coupling. The Ag NWs decoration step was conducted thanks to the polyol reduction of nickel. It allowed producing important amounts of decorated Ag@Ni NWs. The decorated wires were then processed in an intrinsic piezoelectric P(VDF-TrFE) matrix to obtain a magnetoelectric composite. Here we present the magnetic filler fabrication, its morphological and structural characterization obtained by microscopy. The composite structural analysis was conducted; the crystalline amount and the piezoelectric properties were determined. Magnetic and magnetoelectric properties were finally measured to check the influence of aspect ratio over magnetization.

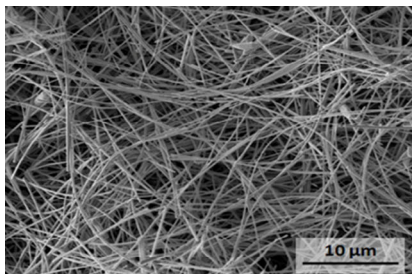
2. Experimental Section

2.1. Materials

Poly(vinylidene fluoride-co-trifluoroethylene) (PVDF-TrFE) was chosen for its intrinsic piezoelectric properties coupled with its easy processing and good resilience. The P(VDF-TrFE) used in this study showed a ratio VDF/TrFE of 70/30. It was provided by Piezotech as a powder. Nickel spherical particles (Ni NPs) with a mean size of 3 μm were provided by Aldrich. Silver nanowires were produced according to previous works.^[25,26] They were washed to eliminate all surface PVP residue and dispersed in 1,2 butanediol. Nickel ions came from hydrated acetate $\text{Ni}(\text{CH}_3\text{COO})_2 \cdot 4\text{H}_2\text{O}$. It was dissolved in 1,2 butanediol, which also acted as reducer. Hydroxyl ions were introduced by an aqueous solution. All chemicals were provided by Aldrich. The materials were used in their as-received state.

2.2. Silver Wire Decoration

Typically, 100 mg of clean silver wires (**Figure 1**) was dispersed in 20 mL of 1,2 butanediol. Separately, 1 g of nickel acetate was dissolved in 30 mL of 1,2 butanediol with 0.1 mol of $\text{NaOH}_{(\text{aq})}$ under magnetic agitation at 800 rpm at 353 K. Once dissolution was complete, the two solutions were mixed together in an ultrasonic bath to homogenize the suspension. This suspension was then put in a round bottom flask immersed in an oil bath. It was heated up to 453 K for 45 min with soft mechanical agitation.



At the end of the nickel reduction, the suspension was filtered and the wires were washed in butanol, ethanol, water, and acetone to remove the polyol residue.

Magnetic decantation was used to remove nonmagnetic particles and wires. The nickel-decorated silver nanowires (labeled “Ag@Ni NWs” on the model of core@shell nomenclature) were observed with scanning electron microscopy (SEM) to determine their aspect ratio. Energy dispersive X-ray spectroscopy (EDS) was used to confirm the presence of nickel over the Ag NWs.

2.3. Composite Processing

Composites were prepared using the solvent-casting method. The typical protocol for the composite processing is as follows: P(VDF-TrFE) powder was dissolved in acetone at 343 K while Ag@Ni NWs were also dispersed in acetone in a separated container. The wire suspension was sonicated to avoid aggregation. The mixtures of the dissolved matrix and metallic wires were mixed together and submitted to ultrasonic agitation for 2 min to produce a homogeneous mixture. The mixture was then quickly precipitated in water to obtain the composite. The precipitate composite was then hot pressed under 1 MPa at 495 K to get films with a thickness of around 100 μm .

2.4. Microscopy Characterization

SEM combined with EDS was performed on particles to determine their morphology and chemical composition. Composites were also observed to evaluate the nanowire dispersion in the matrix. The scanning electron microscope used was a JEOL 7800 Prime coupled with an EDS detector SDD X-Max 80 mm^2 , Oxford Instruments. Observations were performed using secondary electrons mode on an aluminum plot where particles were deposited. To determine the microstructure and structure of these particles, transmission electron microscopy (TEM) imaging was performed using a JEOL JEM 2100 F operated at 200 kV equipped with an EDS analyzer (Bruker SDD Xflash 5030). Diffraction patterns were recorded using selected area electron diffraction (SAED) mode with a 150 nm aperture or a digital diffraction pattern obtained by fast Fourier transform (FFT) of high-resolution TEM (HRTEM) images.

2.5. Dynamic Scanning Calorimetry

The physical structure of the composite was studied by calorimetry. The measurements were made in a Thermal Analysis DSC

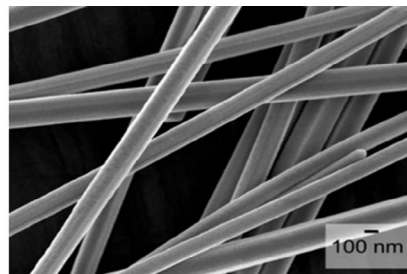


Figure 1. SEM images of pure AgNWs before decoration.

2920 with a heating ramp of 20 K min^{-1} from 353 to 443 K. The crystallinity ratio was calculated with the following equation

$$\chi_C = \frac{\Delta H_C + \Delta H_m}{\Delta H_\infty} \times 100 \quad (1)$$

with χ_C , the crystallinity ratio in percentage, and ΔH_∞ the theoretical value of a theoretical 100% crystallized polymer. In the case of P(VDF-TrFE) ΔH_∞ is equal to 91.45 J g^{-1} . ΔH_C is the enthalpy associated with the Curie transition and ΔH_m is the energy associated with the melting of the crystal.

2.6. Poling Protocol and Piezoelectric Properties

Getting a macroscopic piezoelectricity in composites requires a preliminary poling step. A unidirectional AC electrical field with a sinusoidal shape at 0.1 Hz was applied to the sample placed in castor oil to avoid breakdown. The AC field was slowly increased to 80 MV m^{-1} and maintained for 5 min. The d_{33} piezoelectric coefficient measurements were conducted 24 h after the polarization step to dissipate surface electric charges. The piezoelectric coefficient was measured by a PM 200 piezometer supplied by Piezotest UK. Frequency and stress were set at 110 Hz and 0.25 N, respectively. The stress was applied to the sample in the same direction as the poling field; the polarization was measured to get the d_{33} coefficient.

2.7. Magnetic Property Measurements

Magnetization was measured with a SQUID magnetometer. This technique allows a precision of 1% on the magnetization value. Hysteresis loops were recorded between -5 and 5 T to reach magnetic saturation. These measurements were conducted on raw Ag@Ni wires, commercial nickel nanopowders (Ni NPs), and 2 vol% P(VDF-TrFE)/Ag@Ni NWs and P(VDF-TrFE)/Ni NPs composites. The magnetization was recorded along and across the surface of the composites to observe the magnetic anisotropy.

2.8. Magnetoelectric Measurements

The magnetoelectric properties were analyzed through magnetoelectric current (I_{ME}) measurement. To generate such a current, the samples were placed under an alternative magnetic field (H_{AC}) and a static magnetic field (H_{DC}). The H_{AC} was generated by two Helmholtz coils and supplied by an Agilent signal

supplier link to an audio amplifier. Thus, it allowed controlling of the shape, the frequency, and the intensity of H_{AC} . In this study, ME properties were measured as a function of H_{AC} intensity with a sinusoidal signal at 1 kHz frequency. Samples were thin film shaped with a thickness of $200 \mu\text{m}$. Their surfaces were metalized to avoid contact resistivity. Under the magnetic field, the current generated by the sample was measured by a lock-in amplifier. The magnetic field generated by the Helmholtz coils was measured by a Hall sensor. This measurement permits calculating the ME coefficient α_{ME} using ME theory.^[24] It is obtained with the following equations

$$\alpha_P = \frac{I_{ME}}{H_{AC}} \quad (2)$$

$$\alpha_{ME} = \frac{\alpha_P}{\epsilon_0 \epsilon_r} \quad (3)$$

with α_P the polarization coefficient, α_{ME} the magnetoelectric coupling coefficient, S the surface of the composite, ω the field frequency, H_{AC} the field intensity, and ϵ_r the relative permittivity of the composite.

3. Results and Discussion

3.1. Ag@Ni NWs Properties

3.1.1. Ag@Ni NWs Morphology and Composition

The morphology and aspect ratio of decorated wires were studied by SEM using secondary electron detection mode. The observations are shown subsequently (**Figure 2**) with two different magnifications. The SEM images display wires with homogeneous thickness ($\approx 200 \text{ nm}$). They also show the existence of pseudocubic nodules on the Ag wire surface. At higher magnification, it is clear that the wire surface has been modified as it seems rougher than previously. This roughness is linked with the reduction of nickel ions on the silver surface. Nevertheless, we observe polyhedral nodules on several wires. As these nodules do not exist on the raw silver wires, they are probably made of nickel.

Crystalline defaults on the wires' surface are responsible for the nodule formation. These defaults act as preferential growth sites for the nickel. EDS measurements were conducted to determine the chemical composition of the wires (**Figure 3**).

As shown by EDS, nickel is clearly present on the wires. The aluminum peak is due to the support. The Ag@Ni NWs'

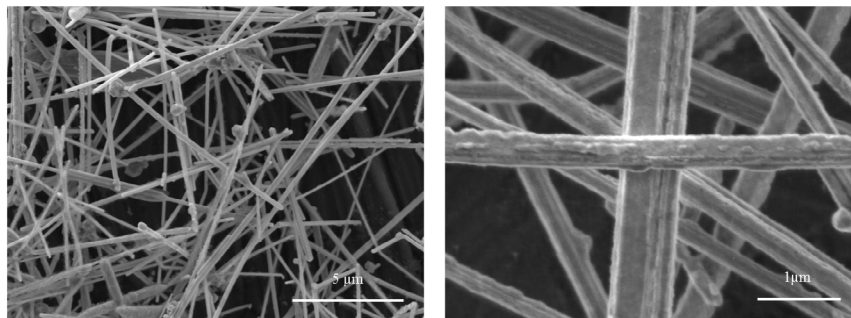


Figure 2. SEM images of Ag@Ni NWs.

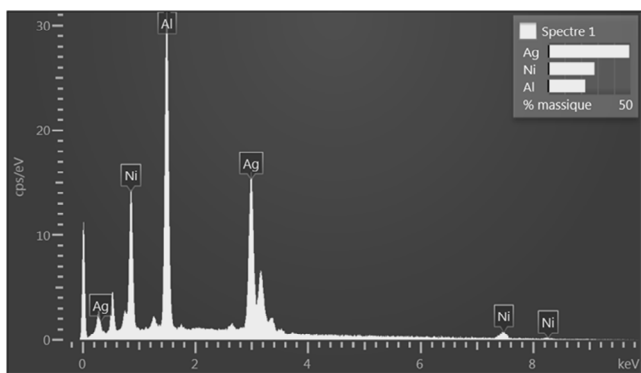


Figure 3. EDS spectrum of Ag@Ni NWs.

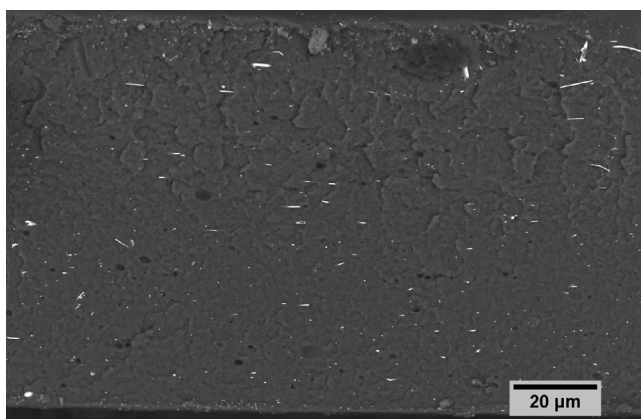


Figure 4. SEM cryocut of P(VDF-TrFE)/Ag@Ni NWs 0.3 vol% composite.

nanotexture was extensively studied by TEM. The wire dispersion in the matrix has also been observed (**Figure 4**). The film was previously cryocut in liquid nitrogen. The SEM micrograph clearly shows the homogeneity of the dispersion. It also shows that the process did not damage the wire's morphology.

3.1.2. Ag@Ni NWs Surface and Texture Analysis

The structure and texture of Ag@Ni NWs have been determined by TEM and HRTEM to characterize the surface layer of the Ag@Ni NWs. First, bright- (BF) and dark-field (DF) images

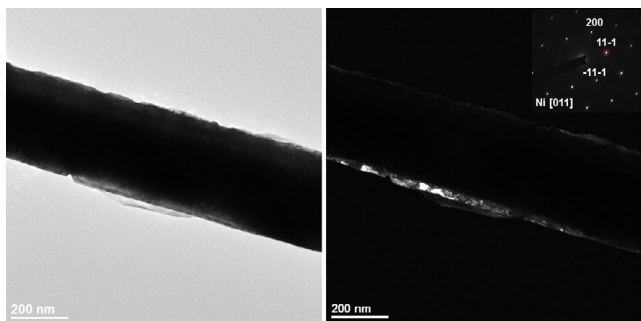


Figure 5. BF (left) and DF (right) images obtained on Ag@Ni NWs combined with the SAED pattern obtained of the surface layer.

(**Figure 5**) were performed. The DF image was obtained using one diffracted spot (red circle) of the SAED pattern obtained on the surface layer of the wire. These DFs highlight the Ni surface layer of the Ag@Ni NWs, which is homogeneous all along the wire. EDS analysis (not shown here) also confirms the nickel composition of the surface layer. The wire exhibits width from 250 and 300 nm. These wires can present cubic nodules at the surface. The formation of such nodules can be explained by the existence of crystal defaults in the Ag NWs. These defaults play the role of preferential reduction sites leading to the formation of a bigger nickel crystal. Clear thin filaments are also observed, particularly in the DF image as they appear white. Such things have already been observed on electrodeposited nickel nanowires.^[27–29] These filaments are made of NiO and are caused by nickel passivation.

Moreover, the structure of the Ag@Ni NWs was also determined by the SAED pattern (**Figure 6**). The SAED pattern confirms that the surface of the wire is composed of metallic nickel (Fm-3 m, $a = 3.6150 \text{ \AA}$) and the interior is made of metallic silver (Fm-3 m, $a = 4.170 \text{ \AA}$).

In this crystalline phase, nickel is ferromagnetic; then we can expect that these wires have good ferromagnetic properties. We can also note that the Ag crystalline structure is not affected by the presence of the nickel layer. To accurately determine the structure of the surface layer, HRTEM was performed combined with two FFTs (one at the extreme surface) (**Figure 7**). The FFT of the extreme surface shows the existence of a passivation layer made of NiO. It was already observed on nanochains obtained by polyol reduction.^[30] The layer thickness is around 10 nm, which is consistent with the previous observation on nickel particles.

3.2. Magnetic Properties

3.2.1. Particles Properties

Magnetic properties of Ag@Ni NWs were measured in a SQUID magnetometer at four isotherms 2, 100, 300, and 400 K. Magnetic hysteresis cycles were recorded between -5 and 5 T for the four isotherms. The different cycles are reported subsequently (**Figure 8**).

Independently from temperature, magnetization describes hysteresis loops specific to a ferromagnetic compound. This ferromagnetism is due to the deposited nickel layer despite its low thickness. Magnetization at saturation (M_S) is 16 emu g^{-1} at 2 K, which is less than the typical value of nickel particles.^[31] This lower value is the consequence of the silver core and the low amount of nickel regarding the entire particles. For the same reason, remnant magnetization (M_r) is also lower than that of nickel particles.

Nevertheless, the H_C values are much higher than the spherical particle one. This enhancement can be explained by two factors. First, the nickel forms a shell around the silver wire, which means that it is a thin film of nickel over a silver core. Thus, this thin-film geometry generates crystalline anisotropy that creates a preferential orientation of the magnetic moment in the nickel layer. Second, the high aspect ratio of the wires also plays an important role in the creation of shape anisotropy. Such anisotropy makes the magnetic moments' orientation easier along the wires, making the moments' reversal harder.

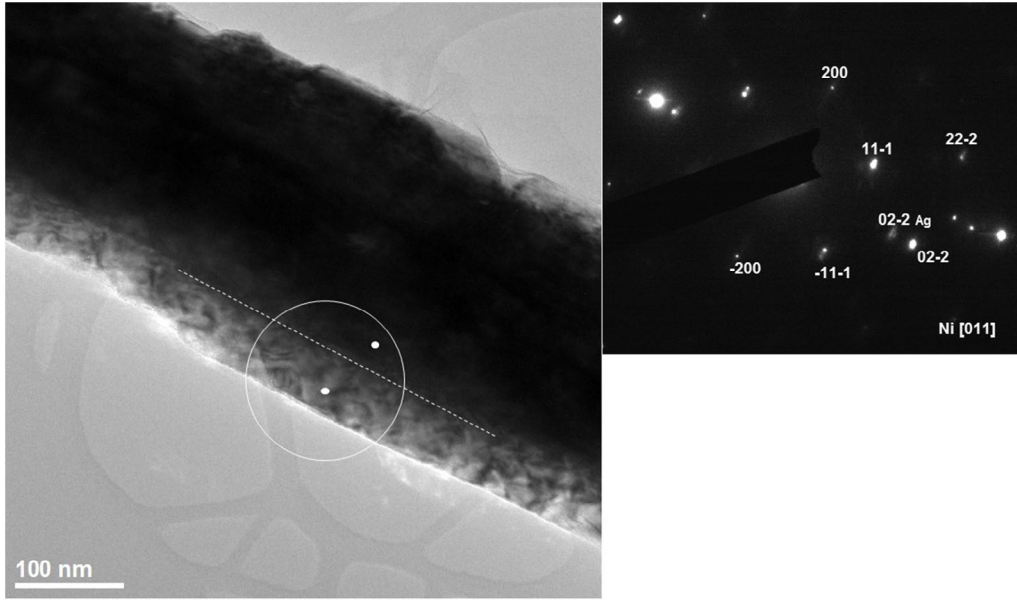


Figure 6. BF TEM image of the Ag@Ni NWs combined with the SAED pattern (the white circle corresponds to the area selected to perform the SAED).

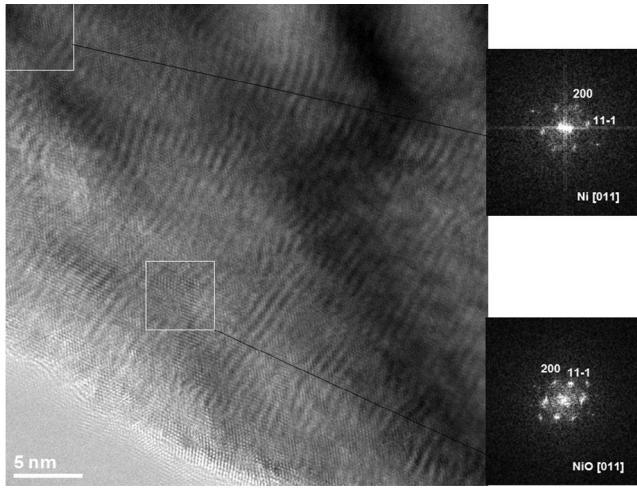


Figure 7. HRTEM image of the surface layer of the Ag@Ni NWs combined with two FFTs.

3.2.2. Composites' Properties

The magnetic properties of P(VDF-TrFE)/Ni NPs and P(VDF-TrFE)/Ag@Ni NWs were measured along and across the film. **Figure 9** shows the evolution of magnetization depending on the applied field in both directions at 300 K.

In both cases, magnetization describes a hysteresis loop showing a ferromagnetic behavior despite the low amount of ferromagnetic particles. In the case of Ni NPs composites, the H_C , M_r , and M_S values are quite similar in the two directions, with $H_C = 90$ Oe, $M_r = 0.4$ emu g^{-1} , and $M_S = 5$ emu g^{-1} . In the case of Ag@Ni NWs composites, we note that the magnetization and coercive field values are dependent on the measurement direction. Measuring along the film surface gives us lower values with

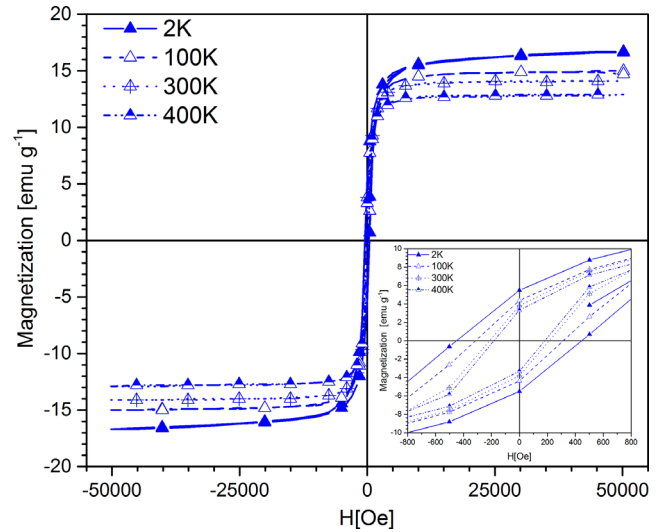


Figure 8. Magnetization cycles for the Ag@Ni NWs at several isotherms.

$H_C = 170$ Oe, $M_r = 0.24$ emu g^{-1} , and $M_S = 2.3$ emu g^{-1} , whereas measuring across the film gives higher values with $H_C = 270$ Oe, $M_r = 0.4$ emu g^{-1} , and $M_S = 2.5$ emu g^{-1} . Thus, it shows clearly the magnetic properties' anisotropy. This anisotropy can be explained by the preferential orientation of the wires along the composite plan reinforced by the Ag@Ni NWs' aspect ratio influence. This orientation is linked to composite processing, i.e., a hot-press process. This phenomenon associated with the particles' aspect ratio has been already observed in the case of nickel nanochains.^[30] Due to the silver core, the magnetization remains lower than that of pure nickel particles. Nevertheless, the aspect ratio has a strong enhancement effect on H_C . For spherical particles and the same amount of nickel, the measured H_C value is 90 Oe.

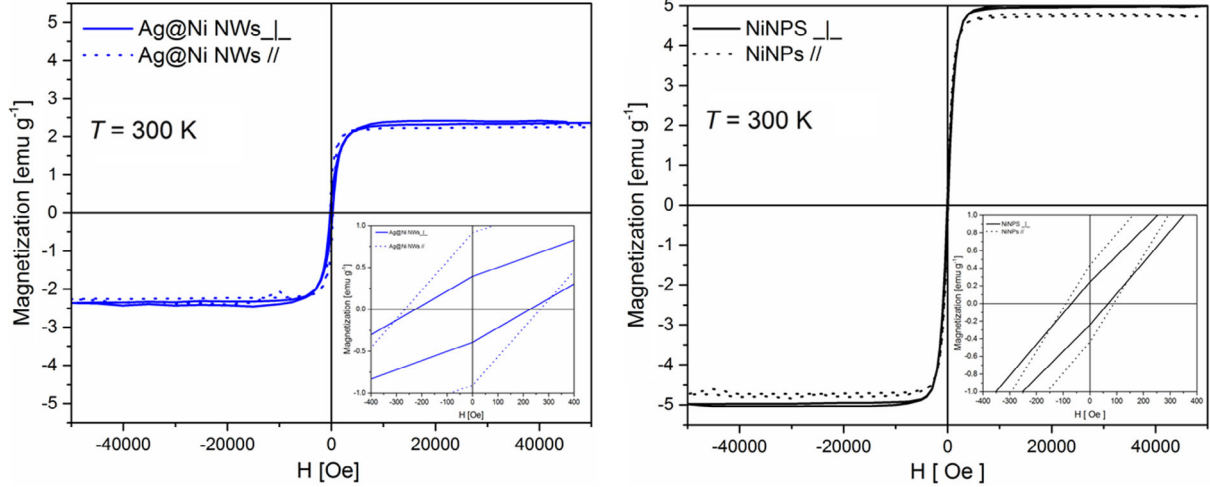


Figure 9. Magnetization of P(VDF-TrFE) composites at 300 K in transverse and longitudinal directions.

3.2.3. Temperature Influence

Four isotherms have been conducted and M_r/M_s values have been reported (**Figure 10**) as a function of temperature for P(VDF-TrFE)/Ag@Ni NWs and P(VDF-TrFE)/Ni NPs composites.

A global tendency is observed; M_r/M_s decreases as a function of temperature. The increasing of temperature allows easier movements of the magnetic moments. Their alignments along the applied field become harder, which makes the M_r lower. The higher is the temperature, the more the magnetization decreases. In the case of Ni NPs composites, the values are low in the two directions. The moments are easier to disorganize due to the lack of aspect ratio and all the morphology effects. It is interesting to note that despite its lower magnetization,

the Ag@Ni NWs composite has the highest value of M_r/M_s in both directions. These values remain high despite the temperature increasing. The stability of magnetic properties in temperature can be explained by the core-shell structure and the particles aspect ratio. In this case, nickel is deposited on silver wires with an important aspect ratio. It means that there is important shape anisotropy. The second cause is the magneto-crystalline anisotropy associated with the fact that nickel is deposited as a layer. These two phenomena make the disorganization of the magnetic moments harder and they do not depend on temperature, explaining the stability of magnetic properties in the case of the Ag@Ni NWs (**Table 1**).

3.3. Physical Structure

The crystalline structure of P(VDF-TrFE) plays a major role in its piezoelectric properties. Thus, it is mandatory to preserve it, more particularly the crystal proportion in the composites. The physical structure has been studied by differential scanning calorimetry at 20 K min^{-1} . Thermograms are shown subsequently (**Figure 11**).

Two thermal events occur on these thermograms. The first event around 373 K is the Curie transition of the β -VDF phase. The second event located around 425 K is the melting of the crystalline phase. The Curie and melting enthalpies were measured by integrating the surface under the associated peaks. The crystallinity ratio was calculated thanks to Equation (1). Calorimetric values for the different samples are reported in **Table 2**.

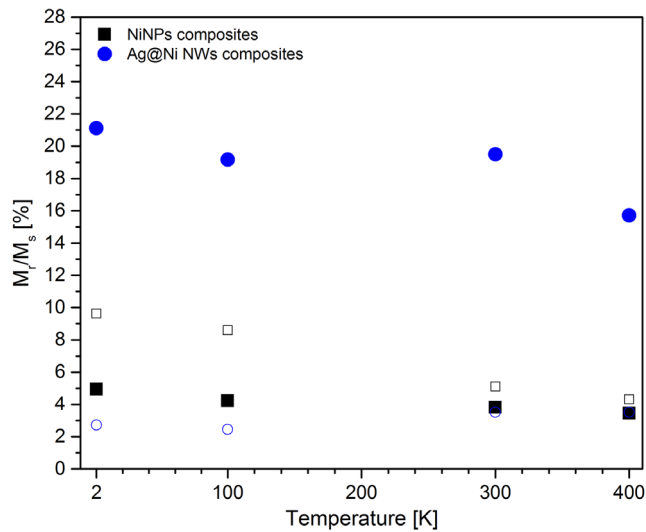


Figure 10. Evolution of M_r/M_s in P(VDF-TrFE) composites depending on temperature in longitudinal (hollow symbols) and transverse (full symbols) directions.

Table 1. Magnetic properties of Ag@Ni NWs.

Temperature [K]	M_r [emu g^{-1}]	M_s [emu g^{-1}]	M_r / M_s [%]	H_c [Oe]
2	5.5	16.6	33	444
100	4.4	15	29	315
300	3.8	14.1	27	211
400	3.3	12.9	26	180

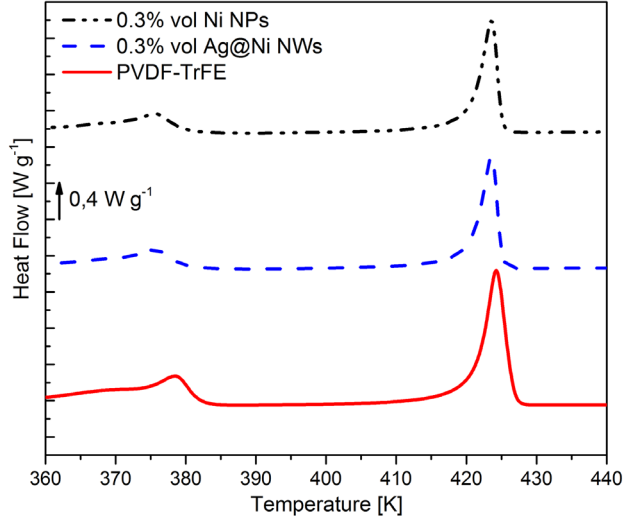


Figure 11. DSC thermograms for P(VDF-TrFE) (red line), P(VDF-TrFE)/0.3 vol% Ni NPs (black line), P(VDF-TrFE)/0.3 vol% Ag@Ni NWs (blue line).

Table 2. Thermal properties of the different samples (reported values of melting ΔH_m , and Curie enthalpies ΔH_C take into account the proportion of metallic fillers in the composite).

	T_C [K]	T_m [K]	ΔH_C [J mol ⁻¹]	ΔH_m [J mol ⁻¹]	χ_c [%]
P(VDF-TrFE)	378.4	424.5	20.4	29.4	54.5
P(VDF-TrFE)/0.3% Ni NPs	375.3	424.2	19.9	28.3	52.7
P(VDF-TrFE)/0.3% Ag@Ni NWs	375.6	423.8	18.9	26.5	49.7

The metallic particle dispersion leads to a small decrease of the melting temperature (T_m), Curie temperature (T_C), and crystallinity ratio (χ_c) compared to pristine P(VDF-TrFE). This phenomenon can be associated with a less organized crystal phase associated with the Ag@Ni NWs. This observation has been already reported in the case of electrodeposited Ni NWs.^[32] T_m values are similar for the three samples. The stability of this value shows that the cohesion in crystallites and their mean size are not affected by the presence of the Ag@Ni NWs at such a volume content. By keeping the volume fraction in wires low, the matrix properties are preserved despite a slow decrease of crystallinity due to metallic particles. Thus, the potentiality of good piezoelectric performance is preserved.

3.4. Piezoelectric Properties

Piezoelectric polymers such as P(VDF-TrFE) require a polarization step to exhibit macroscopic piezoelectric properties. During this step, it is mandatory to reach an electrical field higher than E_C , the coercive field.

In the case of P(VDF-TrFE), this field is $\approx 80 \text{ MV m}^{-1}$. Samples were put in castor oil to avoid electrical breakdown. The electrical field was slowly raised to 80 MV m^{-1} .

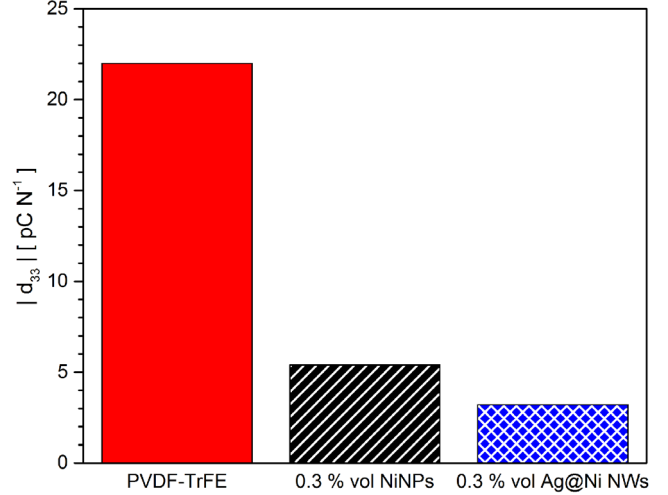


Figure 12. d_{33} values for the P(VDF-TrFE) matrix and P(VDF-TrFE)/Ni NPs and P(VDF-TrFE)/Ag@Ni NW composites.

After 24 h, the piezoelectric d_{33} coefficient was measured. The values are reported subsequently (Figure 12).

Despite the introduction of conductive particles, composites were successfully polarized. An important decrease of the d_{33} value is observed compared to the P(VDF-TrFE) matrix. The reason is twofold: the dielectric losses induced by the conductive particles and the crystallinity ratio decrease. In the case of P(VDF-TrFE)/Ag@Ni NWs, the decrease is more important. This decrease is explained by the Ag@Ni NWs' aspect ratio. The higher aspect ratio has two consequences. First, it increases the dielectrical losses^[33] due to a slightly higher conductivity in the composite, as shown in Table 3. Second, as P(VDF-TrFE) is on the rubbery plateau at room temperature, the Ag@Ni NWs' presence induces additional topological nodes, which increase the rubbery mechanical modulus. It has been previously shown that such modulus increase leads to a transduction/dissipation phenomenon and d_{33} coefficient^[34] decrease. This phenomenon coupled with a lower effective field caused by dielectrical losses and a lower crystallinity ratio explains such a d_{33} decrease.

3.5. Magnetoelectric Properties

Measurements were made under a constant directive magnetic field (H_{DC}) of 4 kOe. The magnetoelectric current (I_{ME}) was measured with a lock-in amplifier and plotted as a function of the alternative magnetic field (H_{AC}). The H_{AC} frequency was fixed at 1 kHz. First, a blank was made with pristine metalized and polarized P(VDF-TrFE) to subtract the environmental noise.

Table 3. Real part of the conductivity for magnetoelectric composites at 0.5 Hz.

Sample	σ' [S m ⁻¹]
P(VDF-TrFE)/0.3% Ni NPs	4.4×10^{-12}
P(VDF-TrFE)/0.3% Ag@Ni NWs	4.9×10^{-12}

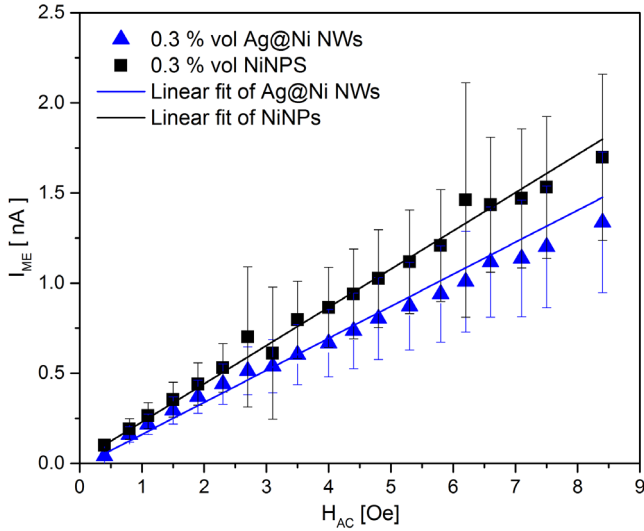


Figure 13. Magnetolectric current for P(VDF-TrFE)/Ag@Ni NW (blue) and P(VDF-TrFE)/Ni NPs (black) as a function of H_{AC} .

The evolution of I_{ME} and its fitting (continuous lines) for the two composites are reported on the following graph (Figure 13).

For the two samples, I_{ME} shows a linear variation with H_{AC} . This linear variation allows us to use a simple equation to determine the coupling coefficient α_{ME} value by applying Equation (2) and (3). The ϵ_r values were measured at 300 K and 1 kHz and are reported in Table 4.

Then, by fitting the evolution of I_{ME} versus H_{AC} we calculated the magnetolectric coefficients of the composites. The α_{ME} calculated values are reported in Figure 14.

In both composites important values of α_{ME} were measured. These values are consistent with the literature for polymer-based composites.^[35] We observe that the Ag@Ni NWs composite exhibits a lower α_{ME} than the Ni NPs composite. Two reasons can explain this difference. First, the d_{33} value measured in the Ag@Ni NW composite is two times lower than in the Ni NP composite. It means that in similar experimental conditions, the recorded I_{ME} will be lower. Second, it has been shown that the magnetic properties of Ag@Ni NWs were lower than those of Ni NPs in terms of magnetization. Thus, the Ag@Ni NWs are less sensitive to the magnetic field, leading to a lower coupling coefficient. Despite the positive effect of the aspect ratio on the magnetolectric coupling, the magnetization and d_{33} are too low to be offset by the aspect ratio. Here, the positive impact of the aspect ratio can be observed through the rather high value of α_{ME} in the P(VDF-TrFE)/Ag@Ni NWs composite despite the low d_{33} and magnetization. Moreover, the results we present here were obtained with a very low amount of magnetic particles, i.e., 0.3%

Table 4. Dielectric permittivity of composites at 1 kHz.

Sample	ϵ_r
PVDF-TrFE	4.2
PVDF-TrFE/Ni NPs	6.8
PVDF-TrFE/Ag@Ni NWs	7.8

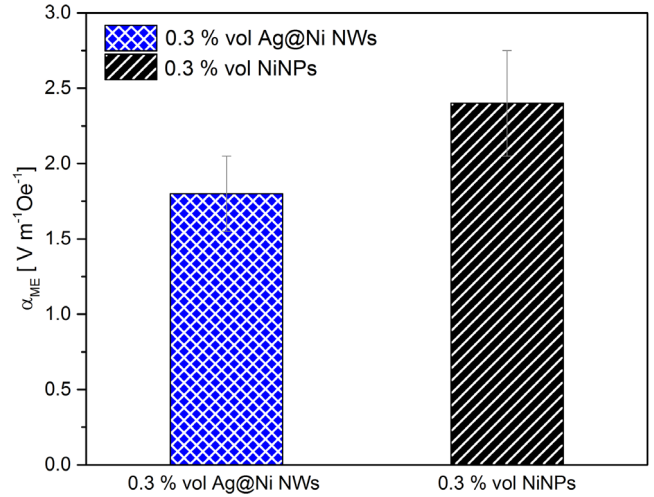


Figure 14. Magnetolectric coefficients of P(VDF-TrFE)/Ag@Ni NWs (blue) and P(VDF-TrFE)/Ni NPs (black).

in volume. Here we confirm the advantage of metallic nickel over most of the ferrites with a higher M_r leading to a better magnetolectric coupling despite the lower filler content. We report in Table 5 some examples of magnetolectric composites with high-aspect-ratio magnetic fillers and a P(VDF-TrFE) matrix. In comparison with Ag@Ni NWs, the use of Ni NWs leads to higher α_{ME} thanks to more important magnetization. But the challenge of Ni NWs elaboration by electrodeposition remains a major drawback for wide application regarding the gain of magnetolectric coupling compared to our solution. Results presented by Policia et al.^[37] show a much higher coupling value with a very high aspect ratio for the magnetic filler and they manage to reach very high piezoelectric coupling. However, several steps of wire alignment and coating are required. Despite the lower values of α_{ME} , our work shows a good compromise between magnetolectric coupling, high-aspect-ratio fillers, and easy processing in terms of magnetic particle elaboration and composite processing.

4. Conclusion

Silver nanowires have been successfully decorated with nickel by a simple polyol process. The nickel layer is homogenous and well crystallized. The 1D morphology is not affected by the process. The nickel thickness is near 80 nm, which allows good magnetic properties for Ag@Ni NWs. Despite a low magnetization, they

Table 5. Magnetolectric properties of several composites.

Composite		α_{ME} [mV cm ⁻¹ Oe ⁻¹]	H_{DC} [Oe]	Reference
Matrix	Filler			
P(VDF-TrFE)	Ag@Ni NWs	18	4000	Our work
	Ni NPs	24	4000	
	Ni NWs	30	2000	[36]
	Fe _{72.5} Si _{12.5} B ₁₅ MW	65	182	[37]

exhibit a high H_C (211 Oe) at ambient temperature and better thermal stability of magnetic properties than nickel spherical particles thanks to the anisotropy effect contribution. Homogeneous/Ag@Ni NWs composites were processed by hot pressing. The magnetic filler amount was fixed at 0.3 vol% to preserve the physical structure of the P(VDF-TrFE) matrix checked by DSC analysis. The P(VDF-TrFE)/Ag@Ni NWs composite was then polarized to obtain a macroscopic d_{33} of 3.2 pC N^{-1} . The magnetoelectric coupling coefficient is equal to 1.8 $V m^{-1} Oe^{-1}$. This value remains lower than a ME coupling obtained with the P(VDF-TrFE)/Ni NPs composite at the same filler rate. Nevertheless, it remains higher than many values reported in the literature for P(VDF-TrFE)/ferrite samples showing a higher amount of magnetic particles. The main advantage of P(VDF-TrFE)/Ag@Ni NWs is the possibility of application in an environment requiring high H_C . Ag@Ni NWs can also be good candidates for the elaboration of three-phased magnetoelectric composites to take advantage of their magnetic properties' thermal stability.

Conflict of Interest

The authors declare no conflict of interest.

Data Availability Statement

Research data are not shared.

Keywords

composites, high aspect ratios, magnetoelectric, nickel, P(VDF-TrFE), silver nanowires

-
- [1] P. Curie, *J. Phys. Théorique et Appliquée* **1894**, 3, 393.
- [2] D. N. Astrov, *Sov. Phys. JETP* **1961**, 13, 729.
- [3] J. Van Suchtelen, *Philips Res. Rep.* **1972**, 27, 28.
- [4] J. van den Boongaard, R. A. J. Born, *J. Mater. Sci.* **1978**, 13, 1538.
- [5] C. Brosseau, V. Castel, M. Potel, *J. Appl. Phys.* **2010**, 108, 024306.
- [6] F. Narita, M. Fox, *Adv. Eng. Mater.* **2018**, 20.
- [7] H. H. Singh, S. Singh, N. Khare, *Polym. Adv. Technol.* **2018**, 29, 143.
- [8] N. Castro, S. Reis, M. P. Silva, V. Correia, S. Lanceros-Mendez, P. Martins, *Smart Mater. Struct.* **2018**, 27, 065012.
- [9] P. Martins, C. M. Costa, S. Lanceros-Mendez, *Appl. Phys. A* **2011**, 103, 233.
- [10] P. Martins, A. C. Lopes, S. Lanceros-Mendez, *Prog. Polym. Sci.* **2014**, 39, 683.
- [11] R. Gonçalves, P. Martins, D. M. Correia, V. Sencadas, J. L. Vilas, L. M. León, G. Botelho, S. Lanceros-Mendez, *RSC Adv.* **2015**, 5, 35852.
- [12] C. W. Nan, M. Li, J. H. Huang, *Phys. Rev. B* **2001**, 63, 144415.
- [13] S. Svirskas, M. Simenas, J. Banyas, P. Martins, S. Lanceros-Mendez, *J. Polym. Res.* **2015**, 22.
- [14] R. Belouadah, L. Seveyrat, D. Guyomar, B. Guiffard, F. Belhora, *Sens. Actuat. A: Phys.* **2016**, 247, 298.
- [15] P. Martins, A. Lasheras, J. Gutierrez, J. M. Barandiaran, I. Orue, S. Lanceros-Mendez, *J. Phys. D: Appl. Phys.* **2011**, 44, 495303.
- [16] C. Behera, R. N. P. Choudhary, *J. Alloys Compd.* **2017**, 727, 851.
- [17] T. H. L. Nguyen, L. Laffont, J.-F. Capsal, P.-J. Cottinet, A. Lonjon, E. Dantras, C. Lacabanne, *Mater. Chem. Phys.* **2015**, 153, 195.
- [18] R. Revathy, A. Kaipamangalath, M. R. Varma, K. P. Surendran, *New J. Chem.* **2020**, 44, 3690.
- [19] B. Martin, E. Dantras, A. Lonjon, C. Lacabanne, L. Laffont, *IEEE Trans. Dielect. Electr. Insul.* **2020**, 27, 1381.
- [20] S. Tang, S. Vongehr, H. Ren, X. Meng, *CrystEngComm* **2012**, 14, 7209.
- [21] Y. Soumare, A. Dakhlaoui-Omrani, F. Schoenstein, S. Mercone, G. Viau, N. Jouini, *Solid State Commun.* **2011**, 151, 284.
- [22] F. Cao, R. Deng, J. Tang, S. Song, Y. Lei, H. Zhang, *CrystEngComm* **2011**, 13, 223.
- [23] Y.-C. Chien, L.-Y. Huang, K.-C. Yang, M. R. Krishnan, W.-S. Hung, J.-C. Tsai, R.-M. Ho, *Emergent Mater.* **2020**, <https://doi.org/10.1007/s42247-020-00108-y>.
- [24] T. H. L. Nguyen, L. Laffont, J.-F. Capsal, P.-J. Cottinet, A. Lonjon, E. Dantras, C. Lacabanne, *Mater. Chem. Phys.* **2015**, 153, 195.
- [25] L. Q. Cortes, A. Lonjon, E. Dantras, C. Lacabanne, *J. Non-Cryst. Solids* **2014**, 391, 106.
- [26] V. Bedel, A. Lonjon, É. Dantras, M. Bouquet, *J. Appl. Polym. Sci.* **2020**, 137, 48700.
- [27] T. H. L. Nguyen, L. Quiroga Cortes, A. Lonjon, E. Dantras, C. Lacabanne, *J. Non-Cryst. Solids* **2014**, 385, 34.
- [28] B. Guiffard, J. W. Zhang, D. Guyomar, L. Garbuio, P.-J. Cottinet, R. Belouadah, *J. Appl. Phys.* **2010**, 108, 094901.
- [29] A. Lonjon, L. Laffont, P. Demont, E. Dantras, C. Lacabanne, *J. Phys. Chem. C* **2009**, 113, 12002.
- [30] B. Martin, E. Dantras, A. Lonjon, L. Laffont, C. Lacabanne, *Phys. Status Solidi A* **2019**, 216, 1900158.
- [31] M. Alagiri, C. Muthamizhchelvan, S. Ponnusamy, *Synth. Met.* **2011**, 161, 1776.
- [32] A. Lonjon, P. Demont, E. Dantras, C. Lacabanne, *J. Non-Cryst. Solids* **2012**, 358, 236.
- [33] H. S. Göktürk, T. J. Fiske, D. M. Kalyon, *J. Appl. Polym. Sci.* **1993**, 50, 1891.
- [34] C. Bessaguet, E. Dantras, C. Lacabanne, M. Chevalier, G. Michon, *J. Non-Cryst. Solids* **2017**, 459, 83.
- [35] P. Martins, S. Lanceros-Mendez, *Adv. Funct. Mater.* **2013**, 23, 3371.
- [36] M. Y. Alnassar, Y. P. Ivanov, J. Kosel, *Adv. Electron. Mater.* **2016**, 6, 1600081.
- [37] R. Polícia, A. C. Lima, N. Pereira, E. Calle, M. Vázquez, S. Lanceros-Mendez, P. Martins, *Adv. Electron. Mater.* **2019**, 5, 1900280.